TECHNICAL REPORT ARCCB-TR-91028

FRACTAL CHARACTERIZATION OF METALLIC FRACTURE SURFACES

L. V. MEISEL

SEPTEMBER 1991

US ARMY ARMAMENT RESEARCH,
DEVELOPMENT AND ENGINEERING CENTER
CLOSE COMBAT ARMAMENTS CENTER
BENÉT LABORATORIES
WATERVLIET, N.Y. 12189-4050

APPROVED FOR PUBLIC RELEASE; DISTRIBUTION UNLIMITED

DISCLAIMER

The findings in this report are not to be construed as an official Department of the Army position unless so designated by other authorized documents.

The use of trade name(s) and/or manufacturer(s) does not constitute an official indorsement or approval.

DESTRUCTION NOTICE

For classified documents, follow the procedures in DoD 5200.22-M, Industrial Security Manual, Section II-19 or DoD 5200.1-R, Information Security Program Regulation, Chapter IX.

For unclassified, limited documents, destroy by any method that will prevent disclosure of contents or reconstruction of the document.

For unclassified, unlimited documents, destroy when the report is no longer needed. Do not return it to the originator.

SECURITY CLASSIFICATION OF THIS PAGE (When Data Entered)

REPORT DOCUMENTATION PAGE		READ INSTRUCTIONS BEFORE COMPLETING FORM
1. REPORT NUMBER ARCCB-TR-91028	2. GOVT ACCESSION NO.	3. RECIPIENT'S CATALOG NUMBER
4. TITLE (and Subtitle) FRACTAL CHARACTERIZATION OF METALLIC FRACTURE SURFACES		5. TYPE OF REPORT & PERIOD COVERED Final 6. PERFORMING ORG. REPORT NUMBER
7. AUTHOR(s) L.V. Meisel		8. CONTRACT OR GRANT NUMBER(s)
9. PERFORMING ORGANIZATION NAME AND ADDRESS U.S. Army ARDEC Benet Laboratories, SMCAR-CCB-TL Watervliet, NY 12189-4050		10. PROGRAM ELEMENT, PROJECT, TASK AREA & WORK UNIT NUMBERS AMCMS No. 6111.02.H610.011 PRON No. 1A05Z0CANMSC
11. CONTROLLING OFFICE NAME AND ADDRESS U.S. Army ARDEC Close Combat Armaments Center Picatinny Arsenal, NJ 07806-5000		12. REPORT DATE September 1991 13. NUMBER OF PAGES 37
14. MONITORING AGENCY NAME & ADDRESS(if different from Controlling Office)		15. SECURITY CLASS. (of this report) UNCLASSIFIED 15a. DECLASSIFICATION/DOWNGRADING SCHEDULE

16. DISTRIBUTION STATEMENT (of this Report)

Approved for public release; distribution unlimited.

17. DISTRIBUTION STATEMENT (of the abstract entered in Block 20, if different from Report)

18. SUPPLEMENTARY NOTES

Submitted to Acta Metallurgica and Journal of Physics D.

19. KEY WORDS (Continue on reverse side if necessary and identify by block number)

Fracture
Fractal
Perimeter-Area Analysis
Perimeter-Yardstick Analysis

20. ABSTRACT (Continue on reverse side if necessary and identify by block number)

Two recent papers have raised serious questions regarding the fractal characterization of metallic fracture surfaces. The results of perimeter-area analysis and the slit island method (SIM), in particular, are cast into doubt. In this report, perimeter-area and perimeter-yardstick analyses of rectifiable curves and of mathematically constructed, simple fractal curves are presented in order to confront some questions raised in open literature. The results also clarify various features of experimental fractal surface analysis.

(CONT'D ON REVERSE)

DD FORM 1 JAN 73 1473 EDITION OF 1 NOV 65 IS OBSOLETE

UNCLASSIFIED

SECURITY CLASSIFICATION OF THIS PAGE (When Data Entered)

20. ABSTRACT (CONT'D)

Although the present analysis cannot unambiguously resolve all the questions raised by the references cited, strong support for the original fractal picture is presented, and techniques for improving the SIM are suggested.

TABLE OF CONTENTS

LIST OF ILLUSTRATIONS

INTRODUCTION

Mandelbrot, Passoja, and Paullay (ref 1) defined the slit island method (SIM), established the fractal nature of fracture surfaces, and reported the negative correlation of fractal dimension D with fracture toughness in a selection of steel alloys in 1984. They also established for the steel samples studied the fractal dimension equivalent (within two percent) determined by SIM and Fourier analysis of fracture surface profiles. Since the publication of Reference 1, SIM has been applied to study metallic fracture surfaces in a number of papers (refs 2-5).

The SIM yields D of fracture surfaces by analyzing the fractal nature of "islands" produced by taking sections (essentially) parallel to the fracture surface. The island perimeter-area relation is used to determine the fractal dimension of the coastline curves, and then Mandelbrot's rule (ref 6) is employed to obtain the fractal dimension of the fracture surface from the coastline fractal dimension. Mandelbrot's rule states that, "...if the section is nonempty, it is "almost sure" that its dimension is D-1...." Exceptions are associated with symmetry axes and are not expected to occur in fracture surface sections.

In this report, with Mandelbrot's rule in mind, we employ the imprecise usage currently in vogue, i.e., we employ the same nomenclature (viz., fractal dimension) and notations (viz., D, D_0, etc.) for fractal dimension of the fracture surface and of the curves bounding the islands produced by sectioning fracture surface and also for the fractional part of the fractal dimension. In addition, we employ the common imprecise nomenclature regarding the definition of fractals, and we refer to objects or mathematical constructs, which scale like a fractal only over a limited range of scales, as fractals.

Two recent publications have questioned the validity of the SIM as a tool for fractal studies. Pande et al. (ref 4) draw a sweeping indictment of the SIM on the basis of some puzzling observations in titanium alloys. Lung and Mu (ref 5) suggest that SIM yields useful information, but does not measure the "intrinsic" fractal dimension D_0. Since sectioning and the perimeter-area relation are basic tools of fractal analysis of surfaces, the implications of these critiques extend beyond fracture surface characterization to diverse areas in meteorology, metallurgy, biology, and geography as described in Reference 7.

Pande et al. studied a series of titanium alloys, employing Fourier analysis of fracture profiles and SIM. Their results raise serious questions concerning the application of SIM and the validity of "Mandelbrot's rule." The D values determined by the two techniques exhibited gross discrepancies: profile Fourier analysis yielded D less than 2.1, while SIM yielded D greater than 2.4. These results (and others associated with perimeter-yardstick studies in the same alloys) led Pande et al. to conclude "...that the slit island method is fundamentally flawed as a measurer of the fractal dimension of a fracture surface."

Lung and Mu contributed a very provocative study of fracture surfaces in steel alloys. Features of their assumptions and theoretical analysis include:

1. Fracture surfaces are "literally" self-similar.

2. There exists a "critical yardstick" value E_0, presumably different for different classes of metals but independent of the fracture toughness, such that for $E < E_0$ the measured fractal dimension D_m exhibits a positive correlation with fracture toughness.

3. If a "small enough" yardstick were employed, SIM would yield the "intrinsic" fractal dimension D_0 (presumably D_0 is Mandelbrot's D).

4. As E decreases, $D_m \rightarrow D_0$, thus, the fracture toughness would show a positive correlation with the intrinsic fractal dimension D_0.

5. Quantitative expressions for the measured fractal dimension at an arbitrary yardstick are derived that are consistent with their steel alloy results and predict an extremely slow approach of D_m (as measured by SIM) to D_0 (= D) as E is reduced for Koch quadric islands.

Features of the experimental results of Lung and Mu for $30CrMnSiNi_2A$ steels include:

1. SIM analysis of fracture surfaces at a yardstick of 1.85 μm is consistent with those usually reported. That is, fractal behavior is observed and the measured fractal dimension exhibits negative correlation with the fracture toughness.

2. SIM analysis of fracture surfaces at yardsticks of 0.08 and 0.15 μm yield measured fractal dimension D_m which show a positive correlation with the fracture toughness.

3. The measured fractal dimension versus yardstick data (shown in their Figure 1) show no sign of convergence.

Based upon their theoretical and experimental results, Lung and Mu concluded that, "...the fractal dimension D_m as determined by the perimeter-area relation is not the intrinsic fractal dimension D_0 of a fractured metal surface..." and that the critical yardstick E_0 lies between 0.08 and 1.85 μm in $30CrMnSiNi_2A$ steels. (Their Figure 1 suggests that E_0 is greater than 0.15 μm.)

Since the negative correlation of fracture toughness with fracture surface fractal dimension reported in all other studies of metallic systems has been extremely difficult to understand, the finding of Lung and Mu that for a "small enough" yardstick a positive correlation of fracture toughness with measured fractal dimension in $30CrMnSiNi_2A$ steels is obtained constitutes an important

discovery. However, Lung and Mu's conclusion that SIM does not measure fractal dimension (even for the 0.08 μm yardstick results in their paper) is quite disturbing.

To address the questions raised in References 4 and 5, and because the perimeter-area relation plays a central role in fractal analysis in general, the principal objective of this report is the formulation of a generalized yardstick-dependent perimeter-area relation. A primary application of the present results, incorporating the earlier discussion of Mandelbrot, Passoja, and Paullay, is to provide an interpretation of the SIM results for metallic fracture surfaces in general and those of Lung and Mu for steel fracture surfaces in particular.

It is also demonstrated that:

1. The standard perimeter-area relation of Reference 1 is valid for "small enough" yardsticks and self-similar fractal curves. That is, the conventional result is obtained in the appropriate limit for self-similar fractal curves.

2. The question of "small enough" yardstick is addressed and discrepancies to be expected at larger yardsticks are discussed.

3. Yardstick-dependent corrections to the perimeter-area relation are derived for Koch fractal curves based upon the "sawtooth" generators of Zhang and Lung (ref 7) and Koch quadric islands.

4. Conventional perimeter-area analysis (as in the SIM) is applied to the numerical evaluation of the fractal dimension of fourth generation Koch quadric islands. The deduced fractal dimension is found to be essentially the intrinsic fractal dimension of the construction (i.e., $D = 1.5$). This finding is consistent with the generalized perimeter-area relation derived here and is inconsistent with the much lower values predicted by the theory of Lung and Mu.

THEORY

The concept of length is central to the discussion of fractals. One requires a yardstick and an algorithm to define and measure lengths. For the ordinary curves of Euclidean geometry, the definitions have the property that the measured length P(E) converges to the "true length" as the yardstick length E decreases. One refers to such curves as rectifiable. However, for the same definitions, the measured length of a fractal curve increases essentially without bound as the yardstick length decreases.

Note that throughout the literature and in this report quantities are represented as smooth continuous functions of E, although, especially at "large yardstick," they vary discontinuously. One thinks of these expressions as holding in a statistical sense or as "smoothed" functions.

Routine Constraint on Yardstick Length

There is a well-known sense of yardstick "too large," which applies to both rectifiable and fractal curves. Consider, for example, measurement of the length of an ellipse, a rectifiable curve. To obtain a good approximation, one must choose a yardstick small, for example, relative to the sum of the distances of a typical point from the foci. Pande et al. in their paper (ref 4) discussed this type of limitation in terms of an outer cutoff for fractal behavior.

The Length-Yardstick Rule

The theory underlying the perimeter-area relation is developed in the context of a simple model: the length of a fractal curve P(E) measured with yardstick E is given by

$$P(E) = F*E^{1-D} \qquad (1)$$

where F and D are constant over the range of yardstick lengths E of interest.

Although F and D may not be strictly constant in practice, Eq. (1) has proved useful in modeling curves found in nature. Mandelbrot (ref 6) credited Richardson with the discovery of this form, identified the exponent D with the Hausdorf dimension, and coined the term fractal dimension for D.

Length and Area Measurement

The length-defining algorithms discussed in this report express the length of a curve at yardstick E as the product of a measurable number N(E) and E, i.e.,

$$P(E) = N(E)E \tag{2a}$$

In such cases, Eq. (1) implies

$$N(E) = F*E^{-D} \tag{2b}$$

Similarly, the area-defining algorithms discussed in this report express the area within a closed curve at yardstick E as the product of a measurable number and E^2. The area within a closed fractal curve is usually implicitly assumed to be essentially yardstick-independent.

"Method A" of Mandelbrot. The Polygon Approximation

The discussion of length in this report is presented in the context of "Method A" of Mandelbrot, which we refer to as the polygon approximation. In the polygon approximation, the length of a curve is measured by setting dividers to an opening E and "walking" them around the curve, yielding an E-dependent length given by Eq. (2a) where N(E) is the number of divider steps. The resulting length is that of an equilateral polygon of side E touching the fractal curve at its vertices. The natural definition of area A(E) at yardstick E is the area of the approximating equilateral polygon. Although this algorithm has not been applied to measure curve lengths (or areas) in the SIM, it is easy

to visualize and yields results equivalent to those given by other algorithms that are computationally easier to implement.

The Box-Counting Algorithm

The algorithms applied in the SIM are equivalent to a "box-counting algorithm," which might be implemented as follows:

1. Superimpose a rectangular grid of spacing E over the island in question.

2. Define N(E), which is the curve length in units of E according to Eq. (2a), as the number of boxes containing a section of coastline.

3. Define the area in units of E^2 of the island as the number of boxes inside the coastline plus half the number of boxes on the coastline.

This form of "box-counting algorithm" is employed in the model calculations reported below; it is equivalent to the methods described in Reference 1 for "small enough" E.

In practice, a box-counting algorithm might be implemented by counting boundary and interior pixels in a digitized image of the fractal curve with the yardstick being simply related to the pixel density. To model such a pixel-counting algorithm, we define N(E) as the number of boxes cut on their lower boundary by the curve in question. We have also applied an algorithm which examines all the box boundaries to determine occupancy and obtained results indistinguishable from those obtained employing the abbreviated algorithm.

Consequences of the Self-Similarity of Fracture Surfaces

Fractal characterization of fracture surfaces is based on the idea that fracture surfaces are statistically self-similar. Self-similarity of the fracture surface implies two types of self-similarity for the "islands" produced in the SIM:

1. The coastlines of the islands are individually (statistically) self-similar. Self-similarity for a given coastline implies that the structure satisfies a scaling condition in the sense that at any given scale the structure can be viewed as a scaled-down (or up) version of the structure viewed at any other scale. Such self-similar curves are fractal and satisfy Eq. (1). (In practice, of course, the range of scales for which self-similarity is obtained is generally limited.)

2. The ensemble of islands is statistically self-similar, and each island can be classified according to its characteristic length L_0. In this context, self-similarity implies that for a given ratio of yardstick-to-characteristic length

$$\epsilon \equiv E/L_0 \tag{3}$$

the ensemble of polygon approximations (corresponding to the ensemble of islands) based upon the appropriate yardsticks, (i.e., $\Xi = \epsilon L_0$ for an island of characteristic length L_0) is statistically similar. The polygon approximations for different L_0 and given ϵ are precisely similar in the case that the islands are strictly self-similar. Here similar is used in the ordinary way familiar from Euclidean geometry.

To describe the self-similar ensemble of islands produced in the SIM, we generalize Eqs. (1) and (2) making the L_0 dependence explicit. For such islands the number of divider steps $N(E,L_0)$ will depend only on ϵ (= E/L_0). Thus,

$$N(E,L_0) = N(\epsilon) = F'\epsilon^{-D} = F'E^{-D}L_0^{D} \tag{4}$$

where the constant F' (= F/L_0^{D}) is independent of E and L_0. Similarly, the coastline length $P(E,L_0)$ of an island having characteristic length L_0 is given by

$$P(E,L_0) = N(E,L_0)E = N(\epsilon)E = F'E^{1-D}L_0^{D} \tag{5}$$

N.b., The polygon approximations of given E or ϵ are not unique.

Therefore, the polygon approximations are not necessarily similar. However, for strictly self-similar curves, similar polygon approximations exist, and it is to these that the discussion literally applies. We are consciously imprecise in this discussion to avoid numerous modifying clauses and because the arguments are essentially correct for the cases where only approximate similarity is obtained.

The Perimeter-Area Relation

The SIM employs the perimeter-area relation to determine the fractal dimension of the slit island coastlines D and hence to determine the fracture surface fractal dimension. Although, as usually implemented, the island perimeters and areas are measured at fixed yardstick E by the box-counting algorithm, we derive the relation in the equivalent polygon approximation at fixed yardstick E here because it is easier to visualize.

In order to derive the perimeter-area relation given in Eq. (5), we need to relate the area to L_0. The area $A(E,L_0)$ of an island having characteristic length L_0 measured with yardstick E is taken as that of the equilateral polygon of side E constructed to evaluate $P(E,L_0)$.

For self-similar islands, polygon approximations of the same ϵ are similar and the area of a polygon approximation of given ϵ is proportional to L_0^2. Thus,

$$A(E,L_0) \equiv G(\epsilon)L_0^2 = G(\epsilon)E^2/\epsilon^2 \qquad (6)$$

where the "area shape factor" $G(\epsilon)$, which depends only on ϵ for a given self-similar shape, is defined in Eq. 6.

Equation (5) can be rewritten at fixed E as

$$P(E,L_0) = F'E^{1-D}L_0^D = C(E)L_0^D = C(E)[E^2/\epsilon^2]^{D/2} \qquad (7)$$

where C(E) is an E-dependent constant. Thus, one may combine Eqs. (6) and (7) to obtain

$$P(E,L_0) = C(E)[A(E,L_0)/G(\epsilon)]^{D/2} \tag{8}$$

Equation (8) provides a theoretical basis for a relation similar to Eq. (1) of Lung and Mu (ref 5).

Since, in conventional perimeter-area analysis one takes twice the slope of the log-log plot of P versus A for fixed E as the fractal dimension and following Lung and Mu, we define the "measured fractal dimension" D_m by

$$D_m/2 \equiv [d\ \ell n(P)/d\ \ell n(A)]_E = [d\ \ell n(P/E)/d\ \ell n(A/E^2)]_E \tag{9}$$

Thus, Eq. (8) implies that

$$\begin{aligned} D/2 &= -[d\ \ell n(P)/d\ \ell n(\epsilon^2)]_E \\ &= -[d\ \ell n(P)/d\ \ell n(G/\epsilon^2)]_E[d\ \ell n(G/\epsilon^2)/d\ \ell n(\epsilon^2)]_E \\ &= [d\ \ell n(P)/d\ \ell n(G/\epsilon^2)]_E[1-d\ \ell n(G)/d\ \ell n(\epsilon^2)]_E \\ &= (D_m/2)\ [1-d\ \ell n(G)/d\ \ell n(\epsilon^2)]_E \\ &= (D_m/2)\ [1-d\ \ell n(G)/d\ \ell n(\epsilon^2)] \end{aligned} \tag{10}$$

where the second, third, and fifth equalities are identities, and the fourth equality follows from the definition of D_m. Of course, the derivatives in Eqs. (9) and (10) are to be evaluated for "smoothed" fits to experimental data, etc.

The fractal dimension actually determined in perimeter-area or perimeter-yardstick analyses shall be denoted D_M in the sequel to discriminate it from the measured fractal dimension D_m defined above and from the intrinsic fractal dimension of the construction or fracture surface D. We shall use the nomenclature "measured fractal dimension" for D_M and D_m. Lung and Mu implicitly assume that $D_M = D_m$; we find that $D_M \leq D_m$ in our analysis.

MODEL CALCULATIONS

Simple closed Koch fractal curves (which are characterized by an initiator, a single generator, having topological dimension D_T equal 1, no fragmentation, etc.) in the plane are discussed in this section. The discussion is restricted

to Koch constructions based on equilateral triangular and square initiators and generators composed of a continuous chain of N equal length line segments. The generators surveyed include that for Koch quadric islands and the "sawtooth" generators discussed by Zhang and Lung (ref 7). The quadric island generator was chosen to allow direct comparison with the theoretical results of Lung and Mu (ref 5) and because the fractal construction is well-known. The sawtooth generators were selected, even though there are problems of self-intersection at advanced generations, because they yield constructions consistent with the relatively sharp angular features and relatively small fractal dimensions typical of metallic fracture surfaces.

Lengths and Areas For the Koch Fractal Curves

It is well-known that for Koch constructions based on generators consisting of N_G equal length elements each reduced in length by a factor r from the previous stage (i.e., the cases discussed here), the fractal dimension of the resulting construction is given by

$$D = -\log(N_G)/\log(r) \tag{11}$$

and that Eqs. (1) and (2), incorporating Eq. (11), define the curve length P(E) and number of segments N(E) at each stage of construction. Furthermore, these Koch constructions are literally self-similar (for the appropriate range of scales), and the "area shape factor" $G(\epsilon)$ is readily obtained.

Equations (6) to (10) provide a basis for addressing the discrepancies to be anticipated between, for example, the measured and intrinsic fractal dimensions for Koch fractal curves. The results obtained for Koch constructions provide simple examples of the implications of the present analysis and, one presumes, insight into the more complex structure of real fracture surfaces.

Scaling For the Koch Constructions

The literal self-similarity implicit in the Koch construction implies that numerical evaluations of P(E,L) from a single island, having unit characteristic length for a selection of yardsticks E ($\equiv \epsilon$), are equivalent to numerical evaluations for fixed E on a selection of islands having a range of characteristic lengths.

One may easily visualize this in the polygon approximation. The number of sides of polygon approximations of a given ϵ are independent of E or L and satisfy

$$N(\epsilon) = N(E,E/\epsilon) = N(\epsilon L,L) = N(\epsilon,1) \tag{12a}$$

Thus,

$$P(E,E/\epsilon) = P(\epsilon,1)E/\epsilon \tag{12b}$$

or

$$P(E,L) = P(\epsilon,1)L = P(\epsilon,1)E/\epsilon \tag{12c}$$

Similarly,

$$G(\epsilon) = A(E,E/\epsilon)[\epsilon/E]^2 = A(\epsilon L,L)/L^2 = A(\epsilon,1) \tag{13a}$$

or

$$A(E,L) = G(\epsilon)L^2 = A(\epsilon,1)L^2 = A(\epsilon,1)(E/\epsilon)^2 \tag{13b}$$

Thus, to model a perimeter-area plot, one does numerical calculations for a single island having unit characteristic length and plots $\log[P(\epsilon,1)/\epsilon]$ ($= \log[N(\epsilon)]$) versus $\log[A(\epsilon,1)/\epsilon^2]$ ($= \log[G(\epsilon)/\epsilon^2]$) for a range of ϵ values equivalent to a plot of $\log[P(E,L)/E]$ versus $\log[A(E,L)/E^2]$ at fixed E for a range of L values. The slope of such plots is given by Eq. (9).

Note that the model fractal curves studied here become rectifiable at some level of elaboration. Thus, the curves become rectifiable for A/E^2 exceeding a value determined by the level of elaboration of the model fractal. The slope of

log[P/E] versus log[A/E²] curves deduced from analysis of these model fractal curves will, therefore, go to ½ for such ranges of log[A/E²]. This sort of constraint on fractal behavior is not expected to be observed in experimental fractal analysis.

Curves Having Constant Area Shape Factor

Equation (10) implies that the "measured" fractal dimension is identical to the intrinsic fractal dimension (i.e., $D_m \equiv D$) when the area shape factor $G(\epsilon)$ is constant. Thus, fractal dimensions measured via the perimeter-area relation D_M will approximate D. Further, for constant $G(\epsilon)$, plots of $\log[P(\epsilon,1)/\epsilon]$ versus $\log[\epsilon^{-2}]$ yield graphs of log[P(E,L)/E] versus $\log[A(E,L)/E^2]$.

Rectifiable curves: the regular decagon. Figure 1 is a plot of the base 10 logarithm (log) of the perimeter determined by the box-counting algorithm in units of the diameter d versus the log of the yardstick in units of d for a regular decagon. Each point is the root mean square (rms) average of the result of 18 random sitings of the measuring grids. The data presented in Figure 1 are "typical" results; the general trend of the data is reproduced, but the individual points, especially in the large E/d region, change for other random sitings. The measured perimeter converges as the yardstick is reduced as expected for a rectifiable curve. (To obtain the "true" perimeter one would have to account for the fact that the average length of a segment cutting through a box is greater than the box side, etc.)

The insert in Figure 1 shows the same data plotted in perimeter-area form. The straight line has slope ½, which is consistent with the fact that D = 1 for a rectifiable curve. Deviations from the line are easily discernible for log[P/E] < 0.8 (i.e., for P/E < 6). Deviation from ideal behavior is more conspicuous in the perimeter-yardstick plot than it is in perimeter-area plot.

The data in the main curve of Figure 1 imply, for example, that a yardstick larger than d/2 or d/10 would be "too large" for 5 or 1 percent rms measurements of P, respectively, for rectifiable curves (based on sets of 18 measurements at a given yardstick).

Essentially the same result is obtained for circles. Similar results are obtained for equilateral triangles, except that at large yardsticks the decrease in the rms P-values is more dramatic and closer to monotonic. Similar yardstick "too large" effects are obtained for fractal curves.

Fourth generation Koch quadric islands. It is well-known that the area of a Koch quadric island is constant at each stage of construction. Thus, the resultant fractal curve contains the same area at all scales. For every new bay observable, a new promontory also comes into view as the scale is refined. (In practice, the number of new bays observed may not equal exactly the number of new promontories observed as E is reduced, etc.) The cessation of the construction at the fourth generation does not spoil the area invariance, but does impose an inside yardstick cutoff on the fractal behavior in a natural way. For $E/L_0 > (1/4)^4 \approx 0.004$, the curve exhibits fractal scaling with D = 1.5; for $E/L_0 < 0.004$, the curve is rectifiable (D = 1) with $P/L_0 = 4[(1/4)^4]^{-1/2} = 64$.

Figure 2 shows plots of natural logarithm (ℓn) of normalized length measured according to the box-counting algorithm versus ℓn of normalized yardstick for two placements of the origins of the measuring grid. (Natural logarithms are employed in Figure 2 to allow more direct comparison with Figures 1 to 3 of Pande et al., in which LOG stands for ℓn.) The straight line, which is not fit to either data set, is that given by Eq. (1) for the fractal part of the construction; it is clearly consistent with the "measured" perimeter-yardstick relation.

Note that as E/L_0 falls below 0.004 in Figure 2, fractal scaling ceases and P/L_0 converges toward 64. That is, the perimeter-yardstick data reflect the fact that the fractal dimension changes from 1.50 to 1.0 as E decreases through 0.004 for the present construction. This situation could be considered in the context of the "tamed coastline" discussion of Mandelbrot (ref 6).

Figure 3 is a plot of the base 10 logarithm (log) of perimeter in units of the yardstick E versus the log of the area in units of E^2 for the fourth generation Koch quadric island. The data shown correspond to $\epsilon > 0.004$, each point is the average of values obtained for 18 randomly selected placements of the measuring grids in the box-counting algorithm, and the calculations are performed by varying E on a single island, having unit square initiator as described above.

The straight line shown is an unweighted least squares fit to the data, yielding a "measured" fractal dimension D_M of 1.45, which is to be compared with the fractal dimension of the construction, i.e., D = 1.50. These results are typical of sets made with 18 random placements of the measuring grids. They are consistent with the theory presented here and with the conventional theory; they are inconsistent with the predictions of the theory of Lung and Mu as contained in their Eq. (12), which would yield $D_m < 1.29$.

If the data for $\epsilon < 0.004$, which correspond to larger A/E^2 values, were shown, then curvature analogous to that in Figure 2 at small ϵ would be seen. This is to be expected since, as previously discussed, fractal behavior ceases (i.e., the curve is rectifiable) for such values of ϵ in fourth generation Koch quadric islands.

Odd element sawtooth constructions: fourth generation, five-element, 110-degree sawtooth triadic islands. It is apparent from their symmetry that the odd element sawtooth generators leave the area invariant at each stage of the

Koch five-element, 110-degree sawtooth triadic islands. For these islands, self-intersection occurs only after the fourth generation. That is, the construction analyzed does not contain self-intersections. The results of 18 individual applications of the box-counting algorithm for random sitings of the grid origin (symbol: +), as well as the rms values at each abscissa (symbol: open square), are shown. One does not see 18 points at each abscissa, since duplicates are common, especially for small $\log[A/E^2]$. The transition to rectifiable behavior apparent for $\log[A/E^2] > 4$ reflects the level of elaboration of the model fractal curve. No systematic deviation from linearity at small $\log[A/E^2]$ is apparent. The measured fractal dimension including all data for $\log[A/E^2] < 4$ is $D_M = 1.162$; by construction $D = 1.134$.

The increased scatter observed at small A/E^2, which corresponds to relatively large ϵ, has nothing to do with fractal behavior and can be understood by considering the application of the box-counting algorithm to the measurement of the length of rectifiable curves seen in Figure 1. The normalized rms deviations associated with the rms values shown in Figures 1, 3, 4, and 6 versus $E/\sqrt{A}$ are essentially scattered about a single curve.

The systematic deviations at large $\log[E/L_0]$, which are apparent in Figure 1, amount to a deviation of only about 0.04 at $\log[E/L_0] \approx -0.04$ (which corresponds to $\log[A/E^2] \approx 0.08$). Thus, such systematic deviations are difficult to see on the scale of variations in Figures 3, 4, and 6.

The data shown in Figure 4 exhibit minimal scatter, but are not atypical results for this particular construction and are representative of results obtained by SIM analysis of odd element sawtooth Koch constructions. The larger (non-systematic) scatter in the rms values at small $\log[A/E^2]$ exhibited in

Figure 3 are toward the other extreme of typical results obtained in the model calculations for constant $G(\epsilon)$ in the present study.

Curves Having Variable Area Shape Factor

Equation (10) implies that the "measured" fractal dimension may deviate from the intrinsic fractal dimension when the area shape factor $G(\epsilon)$ is variable. Thus, the fractal dimension D_M as determined by the perimeter-area relation may differ from the "intrinsic" fractal dimension D. The reliability of the standard technique to determine fractal dimension in the variable $G(\epsilon)$ case is approached via analysis of simple Koch fractals.

In the model perimeter-area calculations, we use the fact that for general $G(\epsilon)$, plots of $\log[P(\epsilon,1)/\epsilon]$ versus $\log[G(\epsilon)/\epsilon^2]$ for a single island (having unit characteristic length) and varying ϵ are equivalent to plots of $\log[P(E,L)/E]$ versus $\log[A(E,L)/E^2]$ at fixed E for an ensemble of self-similar islands of varying L.

Even element Zhang and Lung "sawtooth" islands. The even element generators of Zhang and Lung yield interesting models for slit island bounding curves and provide simple model fractals having variable $G(\epsilon)$. The maximum growth rate of $G(\epsilon)$ with decreasing ϵ is obtained in the case where the Koch construction at each stage applies the outgoing generator to each segment of the previous stage.

Consider the even n element sawtooth generator having tooth angle θ illustrated in Figure 5. The scaling factor r is

$$r = L_m/L_{m-1} = [n \sin(\theta/2)]^{-1} \qquad (14)$$

Thus, for each stage m-1 segment, at stage m the construction produces n/2 new triangular areas equal to

$$Lm^2 \sin(\theta/2) \cos(\theta/2) = [L_0^2 \sin(\theta)/2] [r^2]^m \qquad (15)$$

For each element of length L_0 in the initiator there will be $[n/2]^m$ such triangles at stage m, and thus, the total area growing out of the element of length L_0 in the initiator at stage m is

$$A(m) = [L_0^2 \sin(\theta)/2]\, S_m \tag{16a}$$

where the geometric series S_m is

$$S_m = \sum_{i=1}^{m} [n\, r^2/2]^i = [1-(n\, r^2/2)^m]/[n - 1 - n\cos(\theta)] \tag{16b}$$

and where, recalling that $\epsilon = r^m = L_m/L_0$, one can express A(m) as

$$\begin{aligned} A(m) &= B(n,\theta)\, L_0^2\, [1-(n\, r^2/2)^m] \\ &= B(n,\theta)\, L_0^2\, [1-(n/2)^m \epsilon^2] \\ &= B(n,\theta)\, L_0^2\, [1-\epsilon^w] \end{aligned} \tag{17a}$$

where

$$B(n,\theta) = \tfrac{1}{2} \sin(\theta)/[n - 1 - n\cos(\theta)] \tag{17b}$$

and

$$w = 2 - \log(n/2)/\log[n \sin(\theta/2)] \tag{17c}$$

$$= 2 - [\log(n/2)/\log(n)]\, D \tag{17d}$$

The last equality uses

$$D = \log[n]/\log[n \sin(\theta/2)] \tag{17e}$$

Thus, expressions for $G(\epsilon)$ for outgrowing even n sawtooth constructions can be written down directly. In particular, for square initiator,

$$G(\epsilon) = 1 + 4\, B(n,\theta)\, [1 - \epsilon^w] \tag{18}$$

Clearly, for an ingrowing sawtooth construction, one reverses the sign on the $4B(n,\theta)$ term.

The alternating (increase area, decrease area, etc.) construction is again easy to sum but yields a jumpy $G(\epsilon)$, which is essentially equivalent to a

"noisy" constant $G(\epsilon)$ case (i.e., $d[\ell n(G)]/d[\ell n(\epsilon^2)] = 0$). Similarly, if one orients the even sawtooth generators at random for each segment in the construction, then $G(\epsilon)$ is statistically constant. Note that all the constructions discussed in this section, which are based on even n generators of angle θ, have the same "intrinsic" fractal dimension as given in Eq. (17e).

Even element sawtooth construction: outgrowing, tenth generation, two-element, 140-degree sawtooth triadic islands. Figure 6 presents perimeter-area results for outgrowing, tenth generation, two-element, 140-degree sawtooth triadic islands. For these islands, self-intersection occurs after the sixth generation and the construction analyzed contains self-intersections at approximately one percent of its elements. The results of 18 individual applications of the box-counting algorithm for random sitings of the grid origin (symbol: +), as well as the rms values at each abscissa (symbol: open square), are shown. One does not see 18 points at each abscissa, since duplicates are common especially for small $\log[A/E^2]$.

The line in Figure 6 is least squares fit for values of $\log[A/E^2]$ between 2 and 4.25. As a direct result of the variation of the area shape factor $G(\epsilon)$, systematic deviation from linearity in the rms values of $\log[P/E]$ at small $\log[A/E^2]$ are apparent. (Data for $\log[A/E^2] > 4$ also deviate from linearity reflecting the transition to rectifiable behavior in this tenth generation construction.) The measured fractal dimension including all data is $D_M = 1.060$ for $2 < \log[A/E^2] < 4.25$ $D_M = 1.078$, and by construction $D = 1.099$.

Note the following:

1. Data for $\log[A/E^2] < 2$ would probably be excluded in practical SIM analysis based on the routine yardstick "too large" constraint.

2. The area growth rate with decreasing scale (i.e., decreasing yardstick) for the model discussed is probably unrealistically high for fracture surface

sections. Nevertheless, the error introduced by inclusion of the low $\log[A/E^2]$ data is less than 0.02 for this case.

3. Least squares fits covering a selection of lower cutoffs on $\log[A/E^2]$ would expose the variable $G(\epsilon)$ effect and would allow one to determine $G(\epsilon)$ for the present model.

SUMMARY

1. Perimeter-yardstick data were generally accumulated for Koch constructions and for values of $\log[E/L_0]$ uniformly distributed over values between -0.1 to -3.0. These data are essentially equivalent to SIM data (i.e., perimeter-area data) for values of $\log[A/E^2]$ uniformly distributed over 0.2 to 6.0.

The SIM determinations of D were based on 18 random sitings of measuring grids for each of 20 islands, having $\log[A/E^2]$ between 2 and 4.25.

The model results may be compared directly to experimental SIM results, which are typically based upon roughly 100 islands, having $\log[A/E^2]$ distributed over values between 2 and 5.

2. Fractal dimensions were "measured" excluding yardstick "too large" regions and data at yardsticks so small that the rectifiable nature of the constructs becomes evident. The measured fractal dimensions D_m for all the model fractal curves studied were (within uncertainties inherent in the measurement algorithm) equal to the intrinsic fractal dimensions D of the constructions.

Specifically, the SIM analysis yielded the intrinsic fractal dimension D (= 1.50) for Koch quadric islands, in contrast to the theoretical predictions of Lung and Mu (ref 5).

3. The model fractal islands in the present study become rectifiable (i.e., $D \rightarrow 1.0$) for $\log[E/L_0] < -2.15$, which corresponds to $\log[A/E^2] > 4.25$.

Thus, inclusion of data corresponding to $\log[A/E^2] > 4.25$ yields a lower measured fractal dimension and such data have usually been excluded.

Note that the model data presented here would be correctly interpreted in perimeter-area or perimeter-yardstick analyses:

- Figures 2 and 3 - The data in Figures 2 and 3 were obtained for fourth generation Koch quadric islands rectifiable for $E/L_0 < (1/4)^4$, which corresponds to $\ell n[E/L_0] < 4\ell n[1/4] \approx -5.5$ or $\log[A/E^2] > 8\log[4] \approx 4.8$. The transition to rectifiable behavior is easily observed for $\ell n[E/L_0] < -5.5$ in Figure 2 and could be observed as a distinct change in slope if the data for $\log[A/E^2] > 4.25$ were shown in Figure 3.

- Figure 4 - The transition from fractal to rectifiable behavior near $\log[A/E^2] = 4$ is apparent in the fourth generation, five-element sawtooth perimeter-area data plotted in Figure 4.

- Figure 6 - Although not dramatic (since D_m only changes from 1.08 to 1.00), the transition to rectifiable behavior at large $\log[A/E^2]$ is evident in Figure 6.

- Note that perimeter-yardstick curves for the data presented in Figures 4 and 6 exhibit breaks at appropriate yardstick values, similar to that seen in Figure 2.

Thus, the abrupt changes of D inherent in the Koch constructions studied here are readily detected by casual viewing of perimeter-area or perimeter-yardstick data. A routine mechanical analysis of the model data over various ranges of $\log[E/L_0]$ or $\log[A/E^2]$ could be used to determine both D values.

4. The consequences of yardstick "too large" in the measurement algorithm appear for islands having $\log[A/E^2] < 2$ or $\log[E/L_0] > -1$. A variety of effects can be observed; the primary results may be summarized as follows:

• There is a tendency for the scatter in measured lengths to increase as the yardstick length increases. This is a classical effect and may be observed for rectifiable curves (as illustrated in Figure 1), as well as fractal curves (as illustrated in Figures 2, 3, 4, and 6).

• Perimeter-yardstick plots for the model fractal and rectifiable curves studied here have the form seen at large $\log[E/L_0]$ in the experimental data shown in Figures 1 to 3 of Pande et al. (ref 4). Pande et al. describe this scatter as "...a systematic departure from linearity..." and it comprises part of their indictment of the fractal characterization of fracture surfaces and of the SIM. This "systematic departure" is characteristic of yardstick "too large" length measurements.

• No significant systematic deviation from ideal behavior for $\log[A/E^2] < 2$ is noticeable in SIM analysis of fractal curves having constant shape area factor $G(\epsilon)$.

Consider the data in Figures 3 and 4, which correspond to perimeter-yardstick plots of the form described by Pande et al. The essentially non-systematic, large scatter for these fractal curves at small $\log[A/E^2]$ (which corresponds to large $\log[E/L_0]$) is essentially equivalent to the "scatter" seen on application of the measurement algorithm to rectifiable curves for yardstick "too large" cases as seen in Figure 1.

• Systematic deviations from ideal behavior are easily observable in the small $\log[A/E^2]$ region of rms perimeter-area plots produced by SIM analysis of fractals having relatively strongly scale-dependent areas $A(E/L_0)$. That is, systematic deviations from ideal behavior are observable in the small $\log[A/E^2]$ region of rms perimeter-area plots in the case of fractals having strongly variable shape area factors $G(\epsilon)$. The situation is illustrated for the case of the two-element sawtooth triadic island in Figure 6.

• Supplementing perimeter-area data sets by including $\log[A/E^2] < 2$ data decreases (increases) D_m in variable $G(\epsilon)$ cases for yardstick-dependent area A(E), which increases (decreases) as E is decreased. However, the magnitude of the "error" introduced in the measured fractal dimension D_m is relatively small even for the relatively fast growing islands of Figure 6.

• The systematic deviation from ideal behavior illustrated in Figure 6 is effectively obscured when the raw data (rather than the rms data) are examined. However, of course, the same change in D_m could be detected by least squares analysis of the raw data. (Clearly the same D_m is determined by least squares analysis of the unweighted rms data or the underlying raw data.)

• Typical experimental SIM results exclude data corresponding to yardstick "too large" (i.e., $\log[E/L_0] > 1$ or $\log[A/E^2] < 2$) values. Thus, the classical yardstick "too large" and variable shape area factor effects are negligible in typical experimental SIM analyses.

5. The scatter in perimeter-yardstick data for a given fractal island is inherently (relatively) larger than that in perimeter-area data for an ensemble of self-similar islands. This is apparent in the results of the model calculations undertaken here and can be understood as follows. Consider an ensemble of self-similar curves (island boundaries) of fractal dimension D and a series of measurements, which determine D with a relative error δD from perimeter-area analysis based on a subset of the ensemble and perimeter-yardstick analysis of a particular island. (For the Koch fractal curves described here, this could be the same data set.) Perimeter-area analysis measures D/2, hence the relative error is $\delta D/D$. Perimeter-yardstick analysis measures D-1, hence the relative error is $\delta D/(D-1)$.

To be specific, consider a fracture surface having D = 2.100 with δD = 0.025 so that the slit islands have D = 1.100 and δD = 0.025. Then the relative error in the perimeter-yardstick determined parameter, D-1, is 25 percent, while that for the perimeter-area determined parameter, D/2, is 2.3 percent. Clearly, the perimeter-area plot will be more pleasing to the eye than the corresponding perimeter-yardstick plot.

CONCLUSIONS

1. Pande et al.'s conclusion that the SIM is "fundamentally flawed" is not supported by their data. We respond to their principal criticisms of SIM as follows:

• Although the gross discrepancy in the magnitude of D for the titanium alloy fracture surfaces studied by Pande et al. determined by profile Fourier analysis and by SIM is not understood, it does not indicate that SIM (or Fourier profile analysis) is not reliable.

A possible explanation of the gross discrepancies in the measured D values might be related to the different inherent yardsticks (unspecified by Pande et al.) in the two techniques.

One should not overinterpret the discrepancy. The SIM data presented in Figure 4 of Pande et al. appear to be consistent with a much lower value (essentially of the magnitude determined in their profile Fourier analysis) of D than they derived. Thus, it is possible that the discrepancy is spurious.

At any rate, their SIM-determined fractal dimensions D correlate with their Fourier analysis deduced D and with their measured dynamic tear energy. Thus, it seems that both techniques are measuring dimensional aspects of the fractal nature of titanium alloy fracture surfaces.

• The "...systematic departure from linearity..." at large yardstick values in the perimeter-yardstick data of Pande et al. does not indicate that SIM is not reliable. Their data exhibit the same "intrinsic scatter" and deviations from linearity at larger yardsticks as that seen in the model calculations reported here. We would argue that absence of deviations and "scatter" would have been alarming.

• Pande et al. claim that their titanium fracture surface slit islands are not self-similar. They base this conclusion on the test of self-similarity implicit in the following statement from Reference 4: "We recognize that an essential assumption of this approach is that island shape (say ratio of length-to-breadth) is invariant with size." Since in their titanium alloy fracture surfaces (see their Figure 6) larger islands tend to be skewed least, etc., they conclude that fracture surfaces, in general, are not self-similar.

This line of reasoning is incorrect. Invariance of the "form factor" (= ratio of length-to-breadth) with area is characteristic of similar Euclidean figures, but is not required for self-similar fractal curves. Such invariance is obviously not required for statistically self-similar curves, which one expects to find bounding slit islands. Nor is it required for literally self-similar fractals. To get a feeling for how the results presented in Figure 6 of Pande et al. are consistent with expectations for literally self-similar mathematically-defined fractals, think, for example, of Koch fractals based on a rectangular initiator and a two-element 110-degree sawtooth generator at various scales.

2 Lung and Mu's conclusion that SIM yields measured fractal dimension D_m different from the intrinsic fractal dimension is inconsistent with the model calculations presented here. In particular:

• The theoretical predictions of Lung and Mu concerning D_m for Koch quadric islands were shown to be incorrect. It was shown that SIM yields the intrinsic fractal dimension D (= 1.50) of these constructions for yardstick values at which the theory of Lung and Mu implies that $D_m < 1.30$.

• Even for constructions whose areas vary strongly with scale, relatively small variations in D_m from D are predicted and observed in the present study. These variations could be eliminated by limiting the analysis to islands having $\log[A/E^2] > 2$, i.e., by limiting the analysis to islands satisfying the routine constraint on yardstick length previously discussed in this report, which can be understood in terms of applications of the measurement algorithm to the ordinary curves of Euclidean geometry.

3. Lung and Mu's observation that the measured fractal dimensions D_m of their steel alloys exhibit negative correlation with fracture toughness (in accord with the results obtained in all other metallic fracture studies) greater than 1 μm yardsticks but exhibit positive correlation with fracture toughness at 0.08 and 0.15 μm yardsticks, appears to be an important finding.

4. The variation of D_m with E observed by Lung and Mu is consistent with the discussion of fracture surface fractal structure of Mandelbrot, Passoja, and Paullay (ref 1) and of Mandelbrot's discussion (ref 6) of the variations of fractal dimension with yardstick in his analysis of the length of the coastline of Britain. The multifractal fracture discussion by Williford (ref 8) is also relevant. Based upon the present results and the discussions in References 1, 6, and 8, we hypothesize that the variation of D_m with E reflects a true variation of the intrinsic fractal dimension D of the fracture surface with scale.

As suggested in this report, fractal properties (e.g., D) may be scale-dependent. Thus, yardstick dependence of the sort seen in the model perimeter-yardstick analyses should be detectable in experimental perimeter-yardstick analysis. Yardstick-dependent D should also be observable in experimental perimeter-area analyses performed for a selection of E values and thus, in particular, in SIM studies of fracture surfaces for a range of E.

6. On the other hand, limits on fractal behavior of physical surfaces, curves, etc. are (probably) not governed by the degree of elaboration as in the fourth generation Koch quadric islands discussed here, for example. Thus, the breaks seen in the model perimeter-area plots at large $\log[A/E^2]$ in the present study are not expected to occur in experimental perimeter-area data and, in particular, such changes in slope are not expected to be observed in SIM studies of fracture surfaces.

7. The following modifications of standard SIM procedure are recommended:

- For each island and for the range of yardsticks available, determine rms values (and deviations) of log[P] and log[A] for a selection of sitings of the measuring grids (or pixels, etc.). This might be accomplished, for example, by rotating or repositioning the imaging stage, etc.

- Perform least squares fitting with points weighted according to their rms deviations to determine D.

These modifications make more effective use of an ensemble of islands. For example, they allow one to determine D to a given precision using a smaller number of islands or to determine D to greater precision with a given ensemble of islands. (Clearly these modifications are more important at small $\log[A/E^2]$, where the rms deviations are largest, etc.)

The measuring grids were randomly positioned in the model calculations. Although one must take care not to introduce spurious correlations, it may be more convenient to use a prescribed selection of positions in practical applications.

Performing the measurements for the available range of E values, which is apparently not general practice, is highly recommended in light of Lung and Mu's results. It allows one to detect scale-dependent variations in the fractal dimension and to perform complementary perimeter-yardstick analyses.

The numerical results reported here were obtained for unweighted least squares fits to rms values; only small improvements in the determination of the intrinsic fractal dimension of the fractal constructions were obtained by employing weighted least squares fitting. Thus, although the second modification is recommended, it is judged to be of secondary importance.

REFERENCES

1. B.B. Mandelbrot, D.E. Passoja, and A.J. Paullay, Nature, Vol. 308, 1984, p. 721.
2. E.E. Underwood and K.B. Banerji, "Fractals in Fractography," Mat. Sci. Eng., Vol. 80, No. 1, June 1986, pp. 1-14.
3. Z.Q. Mu and C.W. Lung, "Studies on the Fractal Dimension and Fracture Toughness of Steel," J. Phys. D: Appl. Phys., Vol. 21, No. 5, May 14, 1988, pp. 848-850.
4. C.S. Pande, L.E. Richards, N. Louat, B.D. Dempsey, and A.J. Schwoeble, "Fractal Characterization of Fractured Surfaces," Acta Met., Vol. 35, No. 7, July 1987, pp. 1633-1637.
5. C.W. Lung and Z.Q. Mu, "Fractal Dimension Measured With Perimeter-Area Relation and Toughness of Materials," Phys. Rev. B, Vol. 38, No. 16, December 1, 1988, pp. 11781-11784.
6. B.B. Mandelbrot, Fractal Geometry of Nature, Freeman, New York, 1983.
7. Shou-zhu Zhang and Chi-wei Lung, "Fractal Dimension and Fracture Toughness," J. Phys. D: Appl. Phys., Vol. 22, No. 6, June 14, 1989, pp. 790-793.
8. R.E. Williford, "Multifractal Fracture," Scripta Met., Vol. 22, No. 11, 1988, pp. 1749-1753.

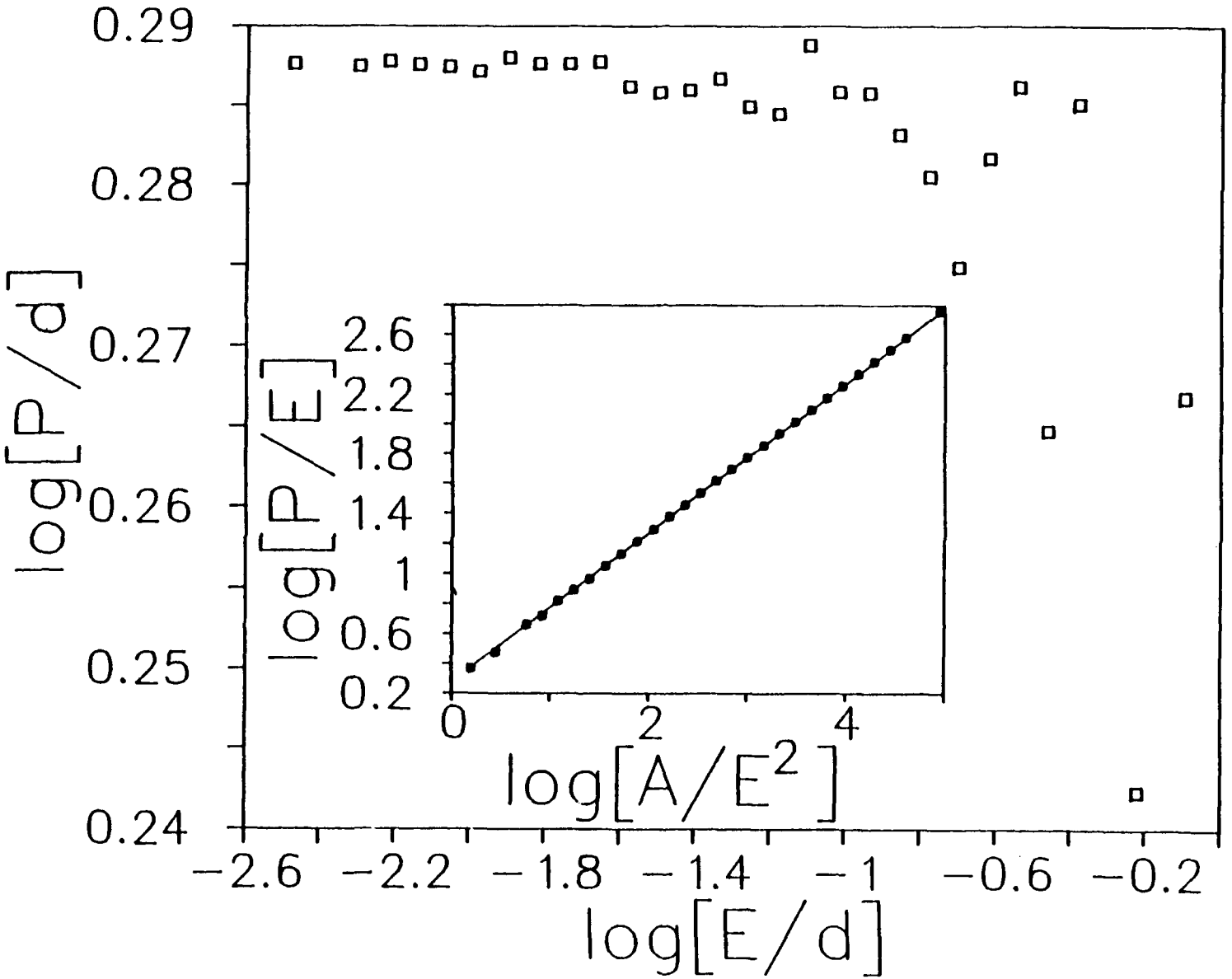

Figure 1. Plot of rms log normalized perimeter versus log normalized yardstick for a regular pentagon of diameter d. The insert shows the same data employed to produce a log normalized perimeter versus log normalized area graph. Each square symbol represents the rms value obtained by analysis based on 18 random sitings of the measuring grids.

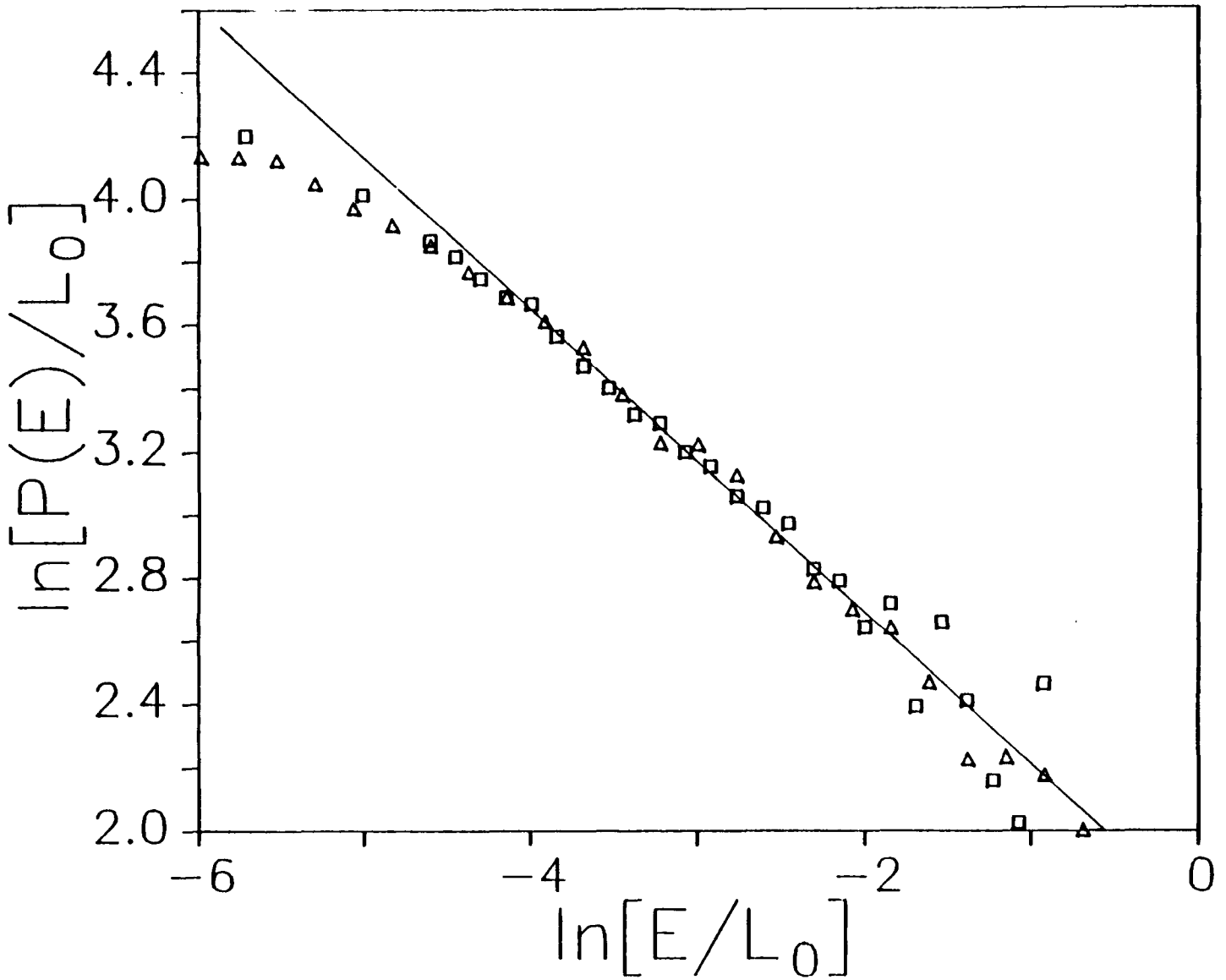

Figure 2. Plots of ℓn normalized perimeter versus ℓn normalized yardstick for two sitings of the measuring grids for a fourth generation Koch quadric island based on an initiator of side L_0. The straight line, which is not fit to the data, has slope -0.5. Natural logarithms were employed to allow direct comparison to Figures 1, 2, and 3 of Reference 4. The break at large negative $\ell n[E/L_0]$ is a consequence of the rectifiable (D = 1) small E limiting behavior of the fractal model. The large scatter for yardstick "too large" is evident.

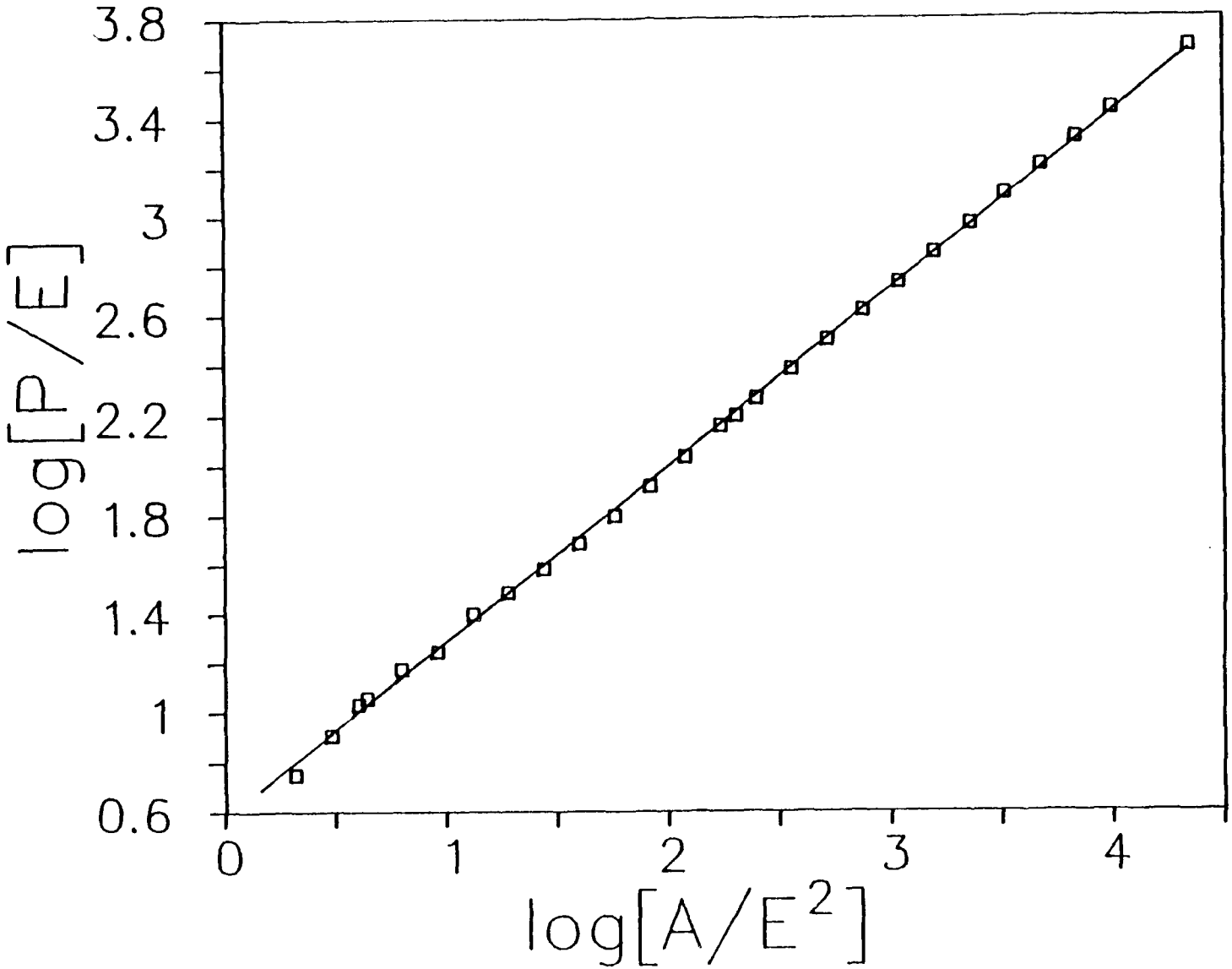

Figure 3. Plot of rms log normalized perimeter versus log normalized area for a fourth generation Koch quadric island. Each square symbol represents the rms value obtained by analysis for 18 random sitings of the measuring grids. The straight line is least squares fit to the data shown.

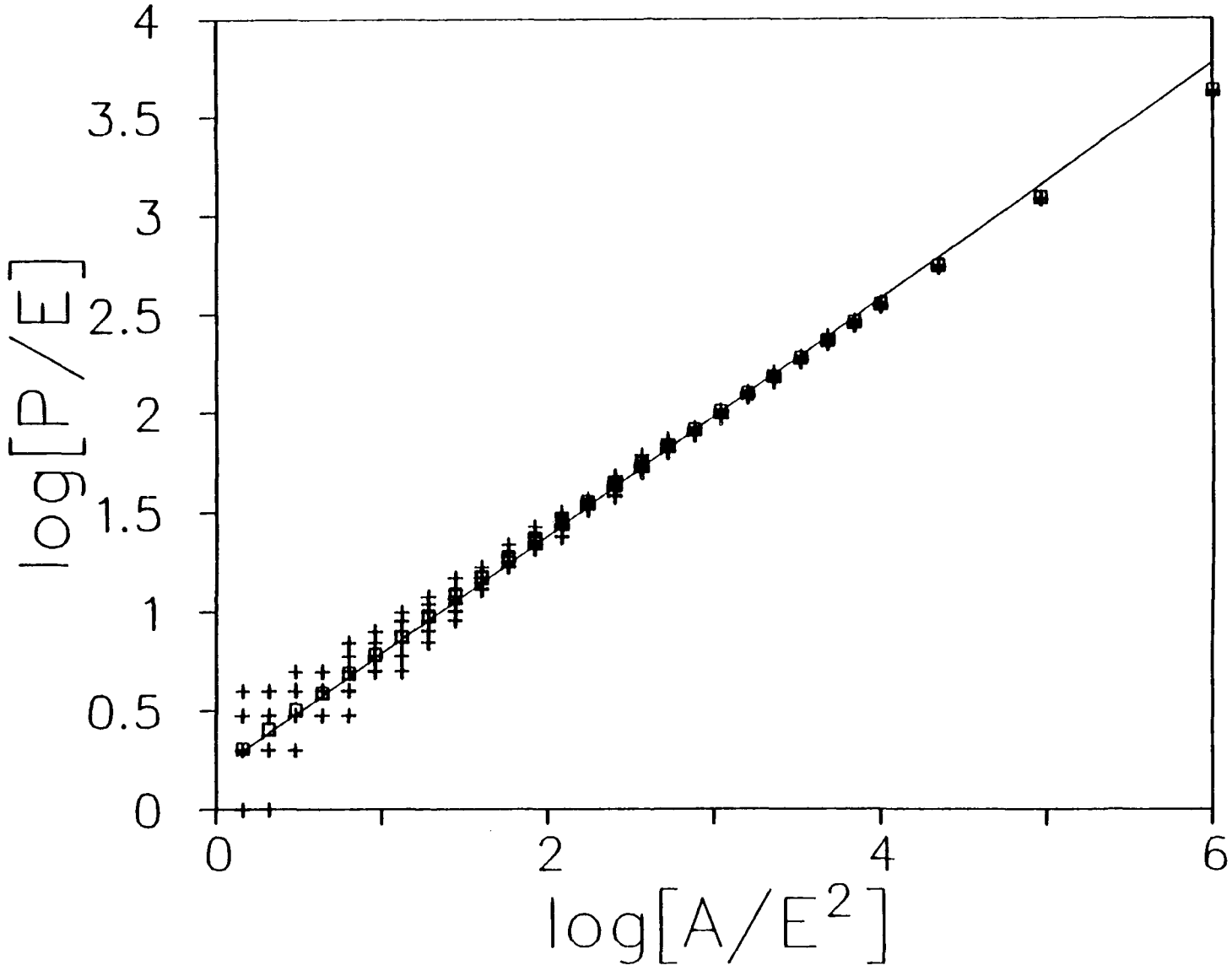

Figure 4. Plot of log normalized perimeter versus log normalized area for a fourth generation Koch triadic island based on a five-element, 110-degree sawtooth generator. Rms values are based on 18 random sitings of the measuring grids at each abscissa. The straight line is least squares fit to the data for $\log[A/E^2] < 4$. The break at $\log[A/E^2] \approx 4$ reflects the fact that elaboration stops at the fourth generation here.

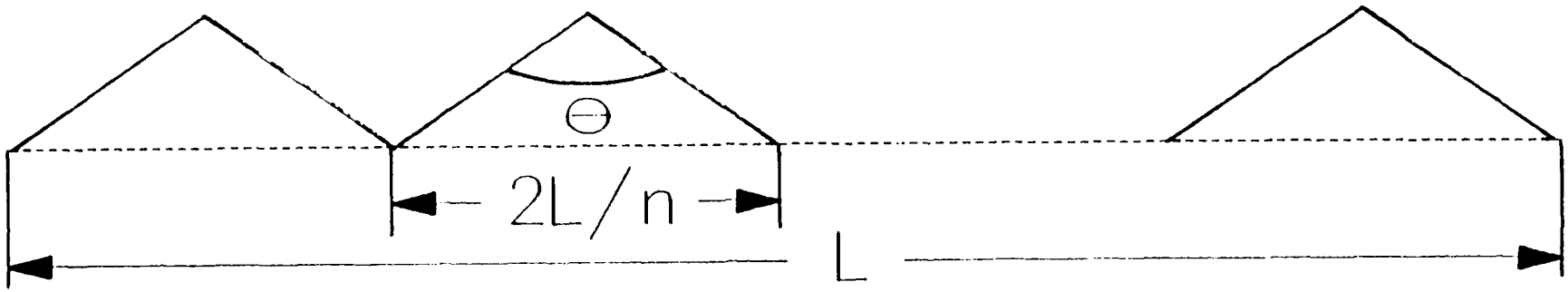

a. The even n sawtooth generator. [n/2] = number of sawteeth.

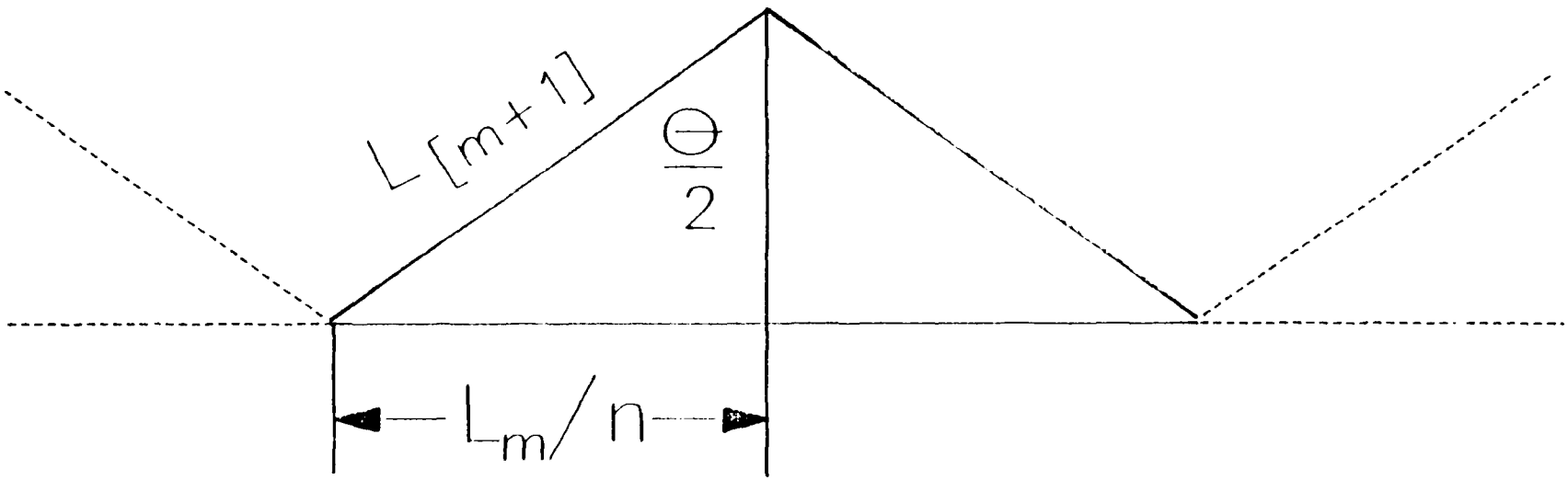

b. Detail of a sawtooth at the $(m+1)^{th}$ generation of construction.

Figure 5

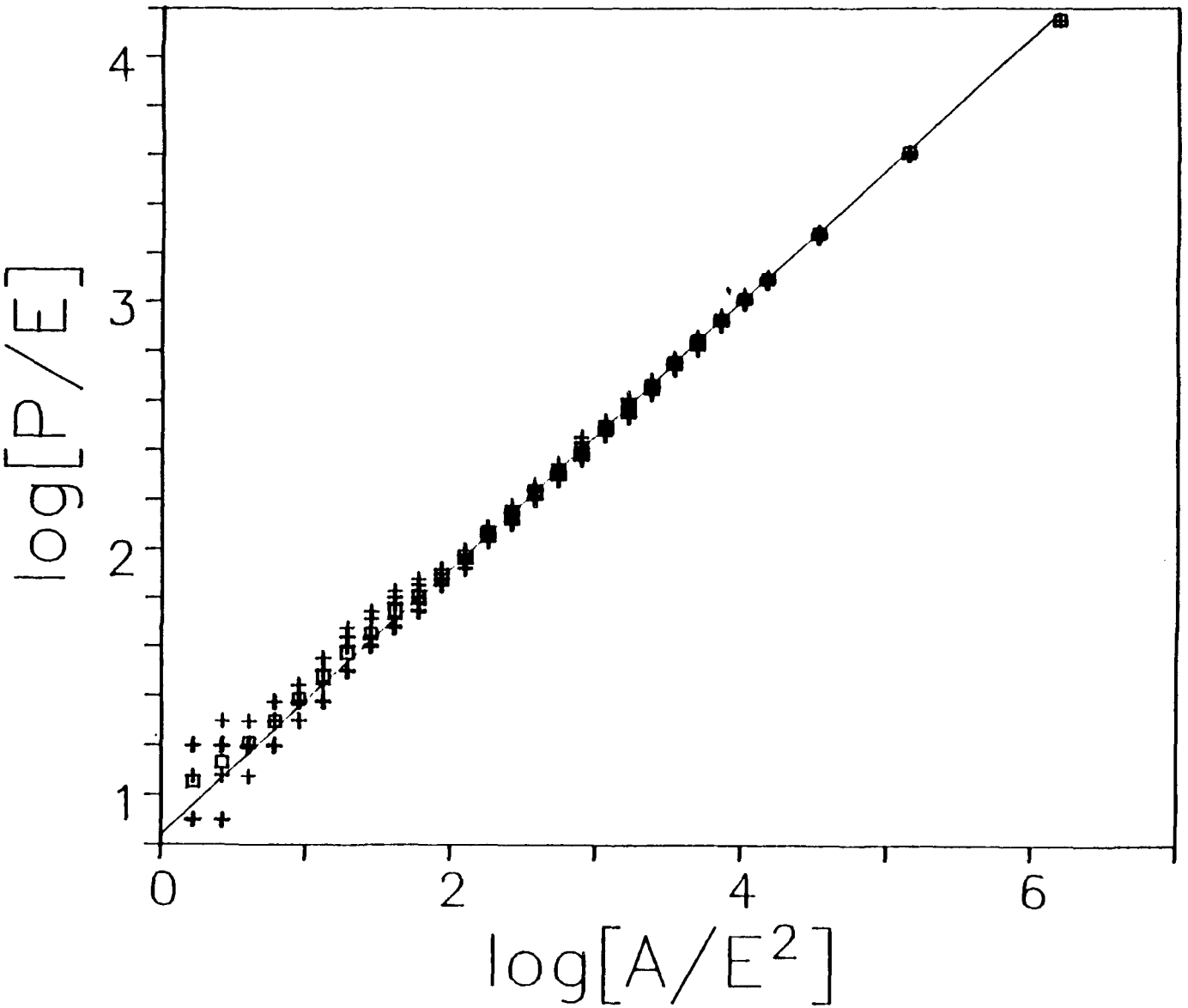

Figure 6. Plot of log normalized perimeter versus log normalized area for a tenth generation Koch triadic island based on a two-element, 140-degree sawtooth generator. Rms values are based on 18 random sitings of the measuring grids. Systematic deviations from the line, which are a consequence of the yardstick-dependent area inherent in the construction, are observed for $\log[A/E^2] < 2$. The small break for $\log[A/E^2] > 4.25$ reflects the fact that elaboration stops at the tenth generation here.

TECHNICAL REPORT INTERNAL DISTRIBUTION LIST

	NO. OF COPIES
CHIEF, DEVELOPMENT ENGINEERING DIVISION	
ATTN: SMCAR-CCB-D	1
-DA	1
-DC	1
-DI	1
-DP	1
-DR	1
-DS (SYSTEMS)	1
CHIEF, ENGINEERING SUPPORT DIVISION	
ATTN: SMCAR-CCB-S	1
-SE	1
CHIEF, RESEARCH DIVISION	
ATTN: SMCAR-CCB-R	2
-RA	1
-RE	1
-RM	1
-RP	1
-RT	1
TECHNICAL LIBRARY ATTN: SMCAR-CCB-TL	5
TECHNICAL PUBLICATIONS & EDITING SECTION ATTN: SMCAR-CCB-TL	3
OPERATIONS DIRECTORATE ATTN: SMCWV-ODP-P	1
DIRECTOR, PROCUREMENT DIRECTORATE ATTN: SMCWV-PP	1
DIRECTOR, PRODUCT ASSURANCE DIRECTORATE ATTN: SMCWV-QA	1

NOTE: PLEASE NOTIFY DIRECTOR, BENET LABORATORIES, ATTN: SMCAR-CCB-TL, OF ANY ADDRESS CHANGES.

TECHNICAL REPORT EXTERNAL DISTRIBUTION LIST

	NO. OF COPIES
ASST SEC OF THE ARMY RESEARCH AND DEVELOPMENT ATTN: DEPT FOR SCI AND TECH THE PENTAGON WASHINGTON, D.C. 20310-0103	1
ADMINISTRATOR DEFENSE TECHNICAL INFO CENTER ATTN: DTIC-FDAC CAMERON STATION ALEXANDRIA, VA 22304-6145	12
COMMANDER US ARMY ARDEC ATTN: SMCAR-AEE	1
SMCAR-AES, BLDG. 321	1
SMCAR-AET-O, BLDG. 351N	1
SMCAR-CC	1
SMCAR-CCP-A	1
SMCAR-FSA	1
SMCAR-FSM-E	1
SMCAR-FSS-D, BLDG. 94	1
SMCAR-IMI-I (STINFO) BLDG. 59 PICATINNY ARSENAL, NJ 07806-5000	2
DIRECTOR US ARMY BALLISTIC RESEARCH LABORATORY ATTN: SLCBR-DD-T, BLDG. 305 ABERDEEN PROVING GROUND, MD 21005-5066	1
DIRECTOR US ARMY MATERIEL SYSTEMS ANALYSIS ACTV ATTN: AMXSY-MP ABERDEEN PROVING GROUND, MD 21005-5071	1
COMMANDER HQ, AMCCOM ATTN: AMSMC-IMP-L ROCK ISLAND, IL 61299-6000	1
COMMANDER ROCK ISLAND ARSENAL ATTN: SMCRI-ENM ROCK ISLAND, IL 61299-5000	1
DIRECTOR US ARMY INDUSTRIAL BASE ENGR ACTV ATTN: AMXIB-P ROCK ISLAND, IL 61299-7260	1
COMMANDER US ARMY TANK-AUTMV R&D COMMAND ATTN: AMSTA-DDL (TECH LIB) WARREN, MI 48397-5000	1
COMMANDER US MILITARY ACADEMY ATTN: DEPARTMENT OF MECHANICS WEST POINT, NY 10996-1792	1
US ARMY MISSILE COMMAND REDSTONE SCIENTIFIC INFO CTR ATTN: DOCUMENTS SECT, BLDG. 4484 REDSTONE ARSENAL, AL 35898-5241	2
COMMANDER US ARMY FGN SCIENCE AND TECH CTR ATTN: DRXST-SD 220 7TH STREET, N.E. CHARLOTTESVILLE, VA 22901	1
COMMANDER US ARMY LABCOM MATERIALS TECHNOLOGY LAB ATTN: SLCMT-IML (TECH LIB) WATERTOWN, MA 02172-0001	2

NOTE: PLEASE NOTIFY COMMANDER, ARMAMENT RESEARCH, DEVELOPMENT, AND ENGINEERING CENTER, US ARMY AMCCOM, ATTN: BENET LABORATORIES, SMCAR-CCB-TL, WATERVLIET, NY 12189-4050, OF ANY ADDRESS CHANGES.

TECHNICAL REPORT EXTERNAL DISTRIBUTION LIST (CONT'D)

	NO. OF COPIES
COMMANDER US ARMY LABCOM, ISA ATTN: SLCIS-IM-TL 2800 POWDER MILL ROAD ADELPHI, MD 20783-1145	1
COMMANDER US ARMY RESEARCH OFFICE ATTN: CHIEF, IPO P.O. BOX 12211 RESEARCH TRIANGLE PARK, NC 27709-2211	1
DIRECTOR US NAVAL RESEARCH LAB ATTN: MATERIALS SCI & TECH DIVISION CODE 26-27 (DOC LIB) WASHINGTON, D.C. 20375	1 1
DIRECTOR US ARMY BALLISTIC RESEARCH LABORATORY ATTN: SLCBR-IB-M (DR. BRUCE BURNS) ABERDEEN PROVING GROUND, MD 21005-5066	1
COMMANDER AIR FORCE ARMAMENT LABORATORY ATTN: AFATL/MN EGLIN AFB, FL 32542-5434	1
COMMANDER AIR FORCE ARMAMENT LABORATORY ATTN: AFATL/MNF EGLIN AFB, FL 32542-5434	1
MIAC/CINDAS PURDUE UNIVERSITY 2595 YEAGER ROAD WEST LAFAYETTE, IN 47905	1

NOTE: PLEASE NOTIFY COMMANDER, ARMAMENT RESEARCH, DEVELOPMENT, AND ENGINEERING CENTER, US ARMY AMCCOM, ATTN: BENET LABORATORIES, SMCAR-CCB-TL, WATERVLIET, NY 12189-4050, OF ANY ADDRESS CHANGES.